J Mater Sci

Metals & corrosion

The role of CSL boundaries for the creep ductility of copper canisters for spent nuclear fuel

Joacim Hagström[1], Rolf Sandström[2,*], and Cláudio M. Lousada[2]

[1] *Swerim AB, Box 7047, 164 40 Kista, Sweden*
[2] *Materials Science and Engineering, Royal Institute of Technology, 100 44 Stockholm, Sweden*

Received: 29 September 2025
Accepted: 7 November 2025

ABSTRACT

The microstructure, grain size and grain boundary (GB) structure of copper in canisters for encapsulation of spent nuclear fuel have been characterized. Coincident site lattice (CSL) GBs were found to be more common than random high angle GBs. Apart from Σ3, the Σ9 and Σ27 GBs show a higher frequency of occurrence than the other CSL GBs. This effect is more pronounced for the material in the canister lid that is slightly deformed. The high fraction of CSL boundaries of 60–65% is of the same order as for grain boundary engineered material. One critical property for the canister is the creep ductility that is improved by the addition of phosphorus (P) to the copper (Cu-OFP). The structure and segregation energies for P onto CSL boundaries have been determined with quantum mechanical calculations. In comparison to a previous study where literature data for the frequency of occurrence of CSL GBs was used, the absolute values of the segregation energies and the occupancy of P at GBs are significantly increased when using data for the canister copper. The presence of P reduces the amount of creep cavitation, which controls the ductility during brittle creep rupture. The creation of cavities and creep ductility are predicted. The computed creep ductility is slightly higher than in a previous study mainly due to the frequent occurrence of the Σ9 GB, which leads to strong segregation of P. The influence of grain size on the creep ductility has also been analysed. A large reduction in ductility with grain size is found for Cu without P which agrees with observations. For Cu-OFP a reduction in creep ductility for grain sizes up to 300 μm is also predicted, but no further reduction is obtained for still larger grain sizes.

Handling Editor: Megumi Kawasaki.

Address correspondence to E-mail: rsand@kth.se

https://doi.org/10.1007/s10853-025-11837-y
Published online: 19 November 2025

Introduction

In FCC materials, the grain boundaries (GBs) are either random high angle boundaries (HAGB) or coincidence site lattice (CSL) GBs. In CSL GBs, atoms in neighbouring lattices are allowed to coincide [1]. To identify the CSL boundaries, they are given a Σ number that is equal to the inverse of the density of coincidence sites. CSL GBs have different properties in comparison to HAGB which influences, for example, grain growth, recrystallization and segregation. With a high fraction of CSL GBs, it has been reported, for example, that corrosion resistance, toughness and creep strength can be improved [2].

This study focuses on both the presence and role of CSL GBs in the copper canister for encapsulation of spent nuclear fuel that will be used in Sweden and Finland. The canisters are large copper tubes (about 5 m in length and 1 m in diameter) and sealed with a lid that is welded to the tube. Both for the canister tube and the lid, Cu doped with 120 at. ppm P (Cu-OFP) is used. Both the creep strength and the creep ductility are improved with additions of P [3, 4]. The latter property is crucial for the integrity of the canister [5]. Phosphorus is present not only in the bulk but also in GBs. The presence of P in GBs has a direct effect on the creep ductility [6]. There is a strong segregation effect of P to specific GBs, and it is vital to know the precise amount for the successful prediction of ductility. It is possible to compute the segregation energies of P (and S) using density functional theory (DFT) [7, 8]. However, the fractions of different CSL GBs in the material must be known so that the most frequent GBs can be modelled, calculations better representing the material can be performed, and more accurate models can be developed.

The purpose of this work is to determine CSL distributions and to perform simulations of the creep ductility in Cu-OFP with special focus on the microstructure of the copper canisters. To be able to perform trustworthy simulations, the microstructure has to be carefully analysed with special attention to the GB distribution. The analyses were done on material from two different canisters. Several different positions from the tube walls and the lid were included. The purpose of the large number of analyses was to gain understanding of the materials homogeneity: large differences in the microstructure at different positions would also imply differences in properties.

There are many studies in the literature on attempts to increase the fraction of CSL boundaries and in this way improve certain properties. A common approach is to apply cold work to 20–30% and then anneal the material in several steps. However, there are many alternatives to this method as detailed in a survey in [9]. After each anneal, the material could be fully recrystallized or the microstructure could only have recovered [9]. The method is commonly referred to as grain boundary engineering (GBE) [10]. GBE has been applied to several materials. Much work has been carried out for stainless steels and superalloys to enhance the corrosion properties, for example, for nuclear applications. Studied alloys include 316 [11], 800H [12], Inconel 600 [13] and Inconel 617 [12, 14]. GBE has been found to reduce intergranular hydrogen embrittlement in pure Ni [15]. Copper has been investigated to improve tensile properties [16]. To raise the ductility, brass has been considered [10]. A range of properties, including intergranular corrosion, cracking and creep, in lead alloys has been analysed [17]. In particular, low stacking fault energy FCC alloys have successfully been tested for GBE [18]. For devising a successful GBE process, microstructure knowledge such as GB distribution is necessary.

This work presents data on grain size and grain boundaries including fractions of CSL boundaries. The data have been evaluated from analysis in a scanning electron microscope (SEM) using electron backscattered diffraction (EBSD). Data from very large areas (> 500 mm^2) through the complete wall thickness (50 mm) were acquired, giving high quality and statistical accurate information. This data is then used in simulations of creep ductility. In a previous study, literature data for the CSL GBs were used [8]. The values for segregation energies and presence of P in GBs in the past and present study are compared, and it is evaluated how they influence the creep ductility. It is also investigated how the grain size affects the creep ductility.

Material and specimens

Material was extracted from the walls of two cylindrical canisters T77 and T101 and from one canister lid. In Table 1, the composition of the canister tubes is listed. This type of Cu is referred to as Cu-OFP. This should be contrasted oxygen-free Cu without P (Cu-OF). Detailed information of the composition of the lid material is not

Table 1 Composition of the investigated tube material in wt. ppm, except for Cu (wt%)

Elem	Cu	P	Ag	Al	As	Bi	Cd	Co	Cr	Fe	H	Mg
T77	99.992	58	13.2	< 0.08	0.4	0.3	< 0.4	< 0.1	0.28	0.6	0.27	–
T101	99.992	45	11.8	< 0.08	1.4	0.7	< 0.4	0.2	0.19	0.7	0.57	< 0.1
Elem	Mn	Ni	O	Pb	S	Sb	Se	Si	Sn	Te	Zn	Zr
T77	< 0.1	1	0.9	< 0.7	4.4	< 1	< 0.7	1.6	< 0.7	< 2	< 0.1	< 0.1
T101	< 0.1	1.9	1.6	< 0.7	6	3	< 0.5	< 0.2	< 0.7	< 2	< 0.1	< 0.1

available, but the general composition is similar [6]. The cylinder was extruded in two steps from a copper ingot. The ingot weight is as high as 12 metric tonnes. The coarse cast structure is broken down during hot working at temperatures above 700 °C to a finer recrystallized microstructure. The lid is forged. The starting piece is a cylindrical block taken from a continuously cast billet. The lid is not fully recrystallized, and some dislocation sub-structure can be found. The two hot-working processes are different in terms of total amounts of strain and stress states. Therefore, the microstructure differs between the tube and the lid.

Ten specimens were manufactured from different positions and section directions with the aim to get detailed information on the materials microstructure and homogeneity. Specimens from radial (equivalent to the thickness direction in the canister wall), tangential and axial directions were fabricated. Two specimens were also taken from the lid. The section directions refer to the normal direction of the analysed surface. The same coordinate system was employed for the lid. Thus, the thickness direction in the lid is the cylinder axial direction in the tube.

Specimens were cuboids with a base of 50 × 30 mm and 20 mm height. The tangential and axial section directions span from the inside to the outside and represent the full wall (and lid) thickness. Wire electrical discharge machining (EDM) (spark machining) was used to extract samples. EDM cutting is made under water, and the material is not heated. Further grinding and polishing steps are explained in "Experimental" section.

Experimental

Electron back scattered diffraction (EBSD) in a scanning electron microscope (SEM) was used to analyse the grain structure. In this way, high spatial and angular resolution (0.1°) can be obtained. The signal comes from an area about 20 nm in diameter. The penetration depth is quite limited, only 2–5 nm. Damage from grinding and diamond scratching must be avoided. To limit the damage, electrical discharge machining was used to extract material from the canisters. Grinding was first carried out with SiC paper (from P320 to P4000). Polishing was then performed with 6 µm, 3 µm, 1 µm and 0.25 µm diamonds in sequence. By combining electropolishing and oxide particle suspension (OP-S), the surface damage was limited. Orthophosphoric acid and water (50/50) were used for electropolishing. The OP-S involved additions of ammonia and hydrogen peroxide (90 ml OP-S, 6 ml ammonia and 4 ml hydrogen peroxide).

A Zeiss GeminiSEM 450 microscope was employed for the EBSD analysis. This instrument can be operated with a high current and small spot. This is essential for high speed EBSD analysis. An Oxford instrument Symmetry EBSD detector that can perform measurements at high speed, > 3000 Hz, was used. Multiple EBSD analyses were combined. The individual areas were 45–48 mm versus 12–15 mm, and the step size was 5 µm. The resulting data sets were about 25–30 million points covering more than 100.000 grains.

During the EBSD analysis, the fraction of non-indexed points was small, less than 2%. The relative angular error between adjacent measurements was low, below 0.1°. The use of the data for evaluation of the CSL boundary fraction was estimated to generate only a small error.

Results for grain boundary structure

Figure 1a–c presents a typical microstructure obtained by EBSD analysis on the canister wall material, in this example from a section in the tangential direction. In Fig. 1a, crystallographic orientations are represented by colours according to an inverse pole figure colour

coding. Grain boundaries are also plotted in Fig. 1a. In Fig. 1b, only grain boundaries are given. Low and high angle grain boundaries as well as CSL boundaries are differentiated by colours and line thicknesses. In Fig. 1c, the Σ3 twin boundaries are removed. Low angle boundaries and random HAGB are dominating. The amount of HAGB (> 10°) was always larger than that of low angle boundaries (LAGB, 2–10°). However, LAGB were more frequent in the lid (20%) than in the canister (3%), since the lid was not fully recrystallized.

Figure 2 shows an analysis through the complete wall thickness including 280.000 grains. It shows that the grain structure is quite homogeneous. Figure 3 presents results from the analysis of CSL boundary fractions in one wall section and one lid section. The differences between the sections were small. The results show that the Σ3 twin boundary was very common in the canister copper; about 50% of the high angle boundaries in the material were of Σ3 twin character. The variation with specimen positions and section orientations in the tube wall was small, 50.5 ± 0.7%. One significant trend was that the fraction of Σ3 was higher close to the canister surface. Another significant difference was that the number of Σ1 (LAGB), Σ9 and Σ27 boundaries was higher in the lid material; this is due to a different fabrication method (forging) and remains of plastic deformation in the lid.

Figure 1 shows that the fraction of CSL boundaries is about 60% for the canister tube and from corresponding figures for the lid (not shown) about 65%. It is interesting to compare these results with GBE processed copper. Coleman et al. [16] found after 25% cold work and a short anneal at 750 °C that the maximum CSL fraction was 68%. The authors performed 5 step processing but the maximum was found already after the second step. Yang et al. [19] carried out single step processing with 5, 10 and 15% cold work and annealing at 400–750 °C. The maximum CSL fraction for each degree of cold work was 77–84%. Randle et al. [20] used 20–40% cold work followed by annealing and reached 62% CSL fraction (only including Σ3, Σ9 and Σ27). It is evident that the CSL fraction in the canister is not very different to what is typically obtained when the material is subjected to GBE processing. These figures are about the same for other materials. Taking the average of the maximum values for the 30 materials in [9], one finds a CSL fraction of 63 ± 15%.

In Fig. 3, Σ9 and Σ27 show higher fractions than the other CSL boundaries. The difference between tube and lid appears primarily for Σ9 and Σ27, which is again due to the presence of a small amount of plastic deformation in the lid. There are theoretical reasons why boundaries of the type $\Sigma 3^{n+1}$ ($n = 1, 2, \ldots$) are more frequent than others [2]. This is explained in some detail in [20, 21]. When two Σ3 meet at a triple point, a Σ9 is easily formed

$$\Sigma 3 + \Sigma 3 \rightarrow \Sigma 9$$

This explains why a comparatively large fraction of Σ9 is formed. When an Σ9 meets an Σ3, the process can continue

$$\Sigma 3 + \Sigma 9 \rightarrow \Sigma 27$$

However, it is still more common when Σ3 and Σ9 meet that a Σ3 is created again

$$\Sigma 3 + \Sigma 9 \rightarrow \Sigma 3$$

These new Σ3 are not necessarily annealing twins, but can form on many planes. This makes them highly mobile, which promotes the interaction between them. This enhances the further development of the fraction of CSL boundaries.

The CLS boundaries are more frequent than other HAGBs. This is illustrated in Fig. 4. When CSL boundaries are left out, the mean grain size increases from about 70 to 200 μm. In a similar way, the high frequency of twin boundaries can be demonstrated as shown in Fig. 5. When the twin boundaries are not included there is a significant increase in the mean grain size.

There was not much variation in the grain size between measured positions. The mean equivalent circle diameter was 68 ± 2 μm in both canister and lid. The maximum measured equivalent circle diameters in canister and lid were 503 and 762 μm, respectively. Further details on the differences between sample positions can be found in a technical report [22].

Modelling of P and S binding energies

Grain boundary models for quantum mechanical modelling

Density functional theory (DFT) computations have been performed to generate segregation energies (ΔE_{seg}) of P and S impurities at relevant GBs. The following GBs are investigated: Σ3(111) [110], 109.5°; Σ5(012) [100], 36.9°; Σ9(2 $\overline{21}$) [110], 38.9° and Σ11(1 $\overline{1}$ 3) [110], 129.5°. Since similar GBs have been analysed

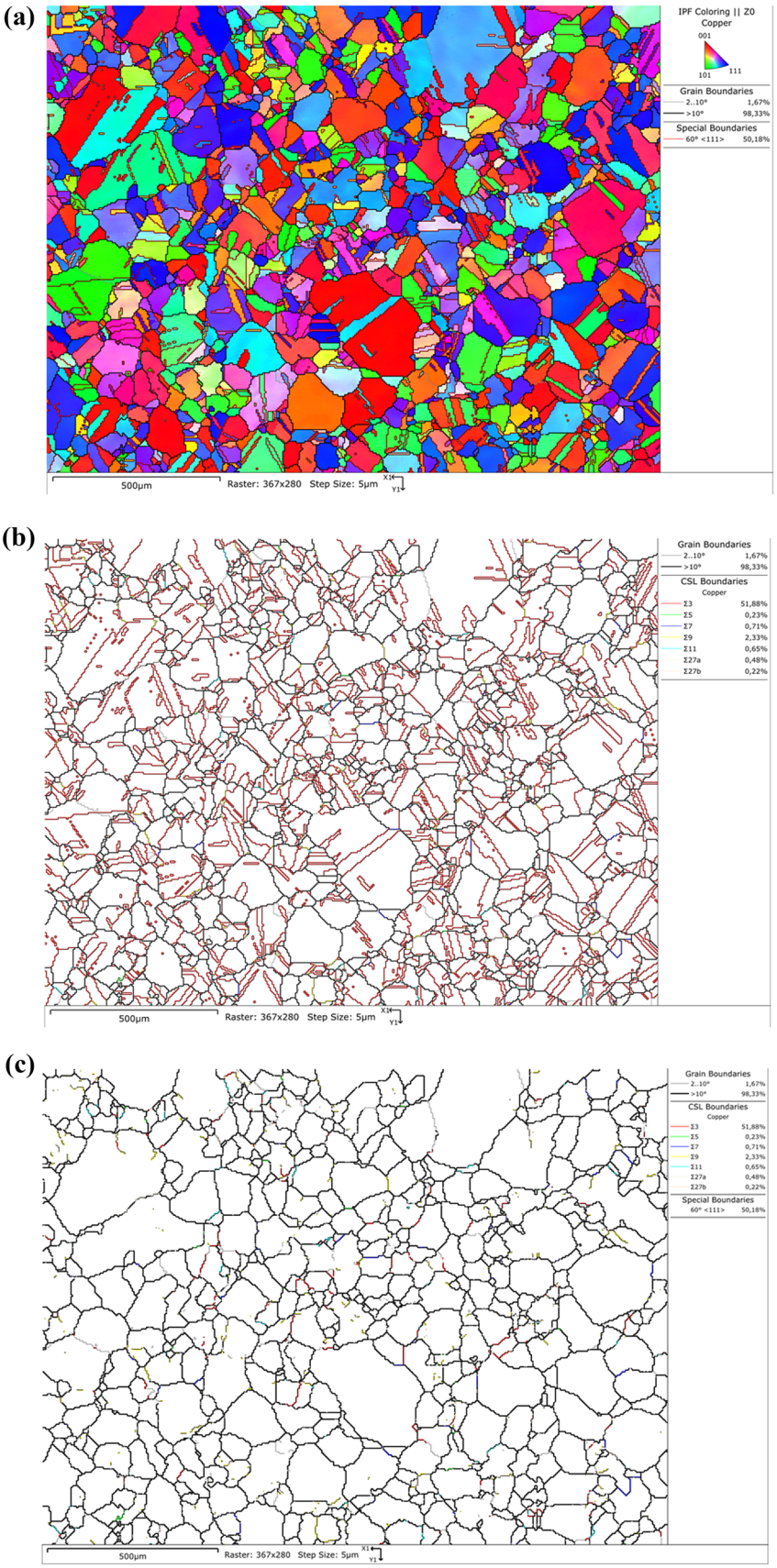

Figure 1 EBSD data from one single EBSD map (from a wall in tangential direction) plotted in three ways. The analysis used 5 µm step size and was built up from 367×280 individual point analyses. **a** Crystallographic orientations plotted using colours according to the inverse pole figure (IPF) in the analysed section normal direction (equals the wall tangential direction). **b** CSL grain boundaries including the 5 first CSL's, and Σ27 which were more frequent than other high Σ boundaries. In **c**, the Σ3 boundaries were "hidden" to visualize how large the grains become if the common 60°<111> boundaries are not considered.

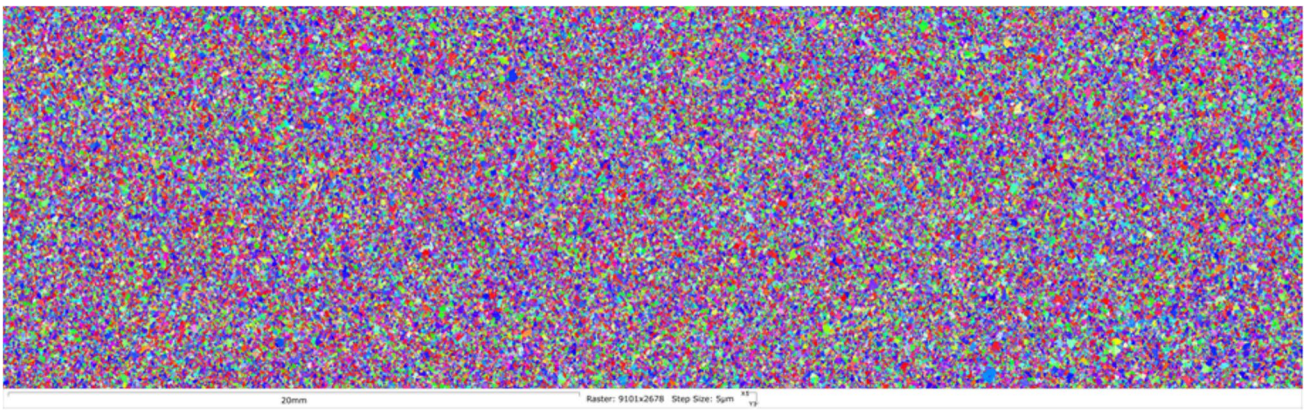

Figure 2 EBSD large area crystal orientation map analysed on a section in the wall with the normal direction in the tangential direction. The analysed area was 45 mm (X) and 14 mm (Y). The step between each analysed pixel was 5 µm giving 24.4 million pixels and about 280.000 grains.

Figure 3 Example of CSL distributions. Fractions of CSL boundaries for canister (tube) and lid. The fraction of Σ3 is about 50%.

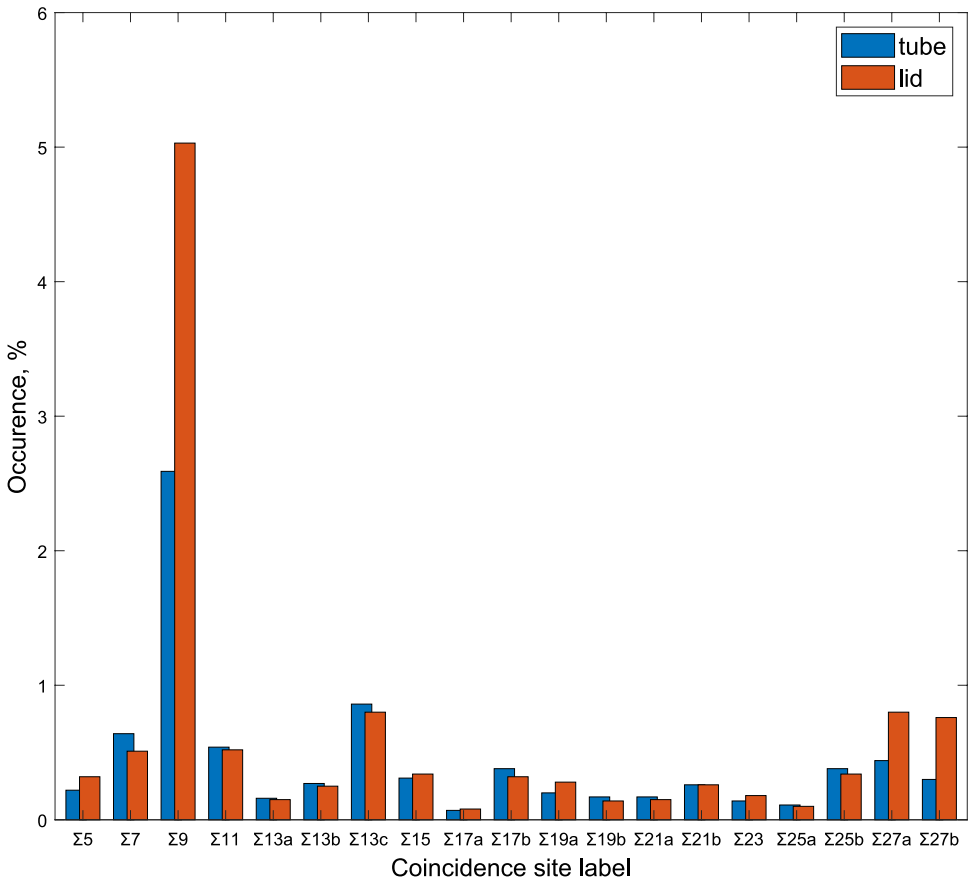

before and presented in previous publications, only a brief summary of the basic assumptions will be given here. The ΔE_{seg} is defined as the difference in binding energy for an impurity atom at or close to GB and the corresponding value in the bulk. Stronger segregation is a consequence of a more negative value of ΔE_{seg}. Further details of the DFT calculations, of the modelling parameters and their benchmarks can be found in our previous work [7, 8, 23–25].

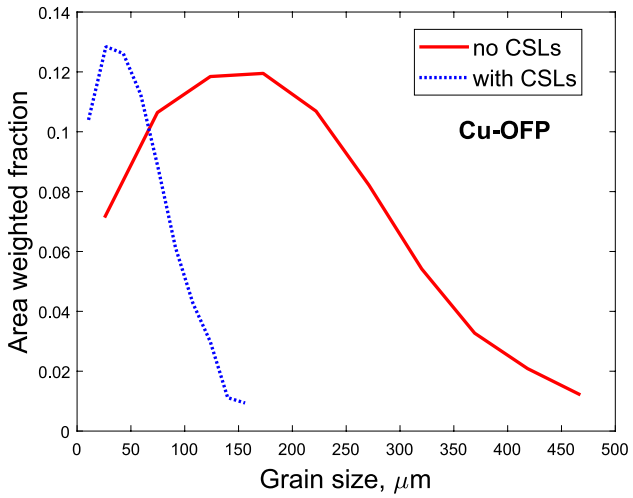

Figure 4 Grain size distribution as area weighted fraction versus equivalent circle diameter from the top-sealing lid in the axial direction. The graph gives distributions without and with CSL boundaries.

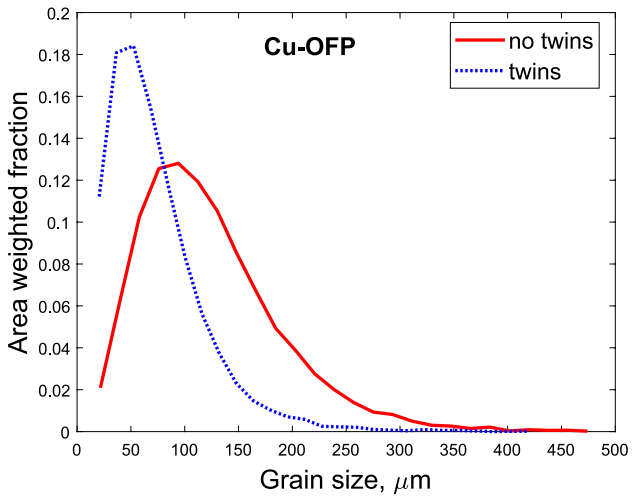

Figure 5 Grain size distribution as area weighted fraction versus equivalent circle diameter from the canister in the axial direction. The graph gives distributions without and with twin boundaries.

The crystallography of Σ3, Σ5, Σ9 and Σ11 is illustrated in Fig. 6. The crystallography was also analysed in [7, 8]. The absorption of P and S was investigated at the labelled substitutional sites in Fig. 6.

Two conditions were used for the selection of these GB models: how often they appear in the material according to the results shown in Fig. 3, and the openness of the GB atomic sites. The excess volume is a key parameter for the segregation of impurities [23–25] and larger excess volumes of GBs are associated with more open GB structures. Σ5 and Σ9 have an open structure, which results in a considerable excess volume for these GBs. All the structural details can be found in previous publications [23, 25].

The construction of the GB models was based on the coincidence site lattice (CSL) method where a GB is modelled using a periodic supercell with two oppositely oriented tilt crystals. CSL works well for establishing periodic GB models, in particular with frequent coincidence sites at the GB plane [26, 27]. After construction of the models, these were optimized following a sequence of supercell optimization and optimization of the atomic coordinates for the previously optimized supercell as previously detailed. Further details of the optimization can be found in [8, 24].

Segregation energies to the GBs

The ΔE_{seg} values calculated with DFT for P and S atoms in the Cu GBs are listed in Table 2. The type of GB (Σ9) is shown in column 1. In column 2, the atomic sites highlighted in Fig. 6 are given. A pair indicator is given in column 3. It takes the value 1 if the atom is on the GB, otherwise 2 to indicate that the value should be computed twice due to the existence of two mirror images of the site on each of the grains. The segregation energies are found in column 4 and 5, the atom coordinates in column 6–8 and finally the distance from the GB in column 9. The coordinate is defined in the following way: the z-axis is perpendicular to the GB plane; the x and y-axes are in the GB in the plane of observation [8].

Both the ΔE_{seg} and their variation with distance from the GB plane follow trends that we have previously observed for similar GBs [8, 23, 24]. For distances up to ≈ 4 Å, the ΔE_{seg} values in Table 2 and in Table 1 in [8] are all negative for S atoms and for all except three positions for P. Thus, there is in general segregation to these GBs. The absolute ΔE_{seg} for S atoms are larger than for P atoms which means that the driving force for segregation of single S atoms is larger than for single P atoms. A similar effect was found for pairs of these impurities [24]. This is consistent with the strength of the chemical bonds between these two elements and Cu atoms in configurations with lower symmetry than that found in substitutional positions of FCC single crystals of Cu [24, 28]. The electronic structure details of the bonding between these impurities and Cu were described in our recent work [24]. In general, the driving force

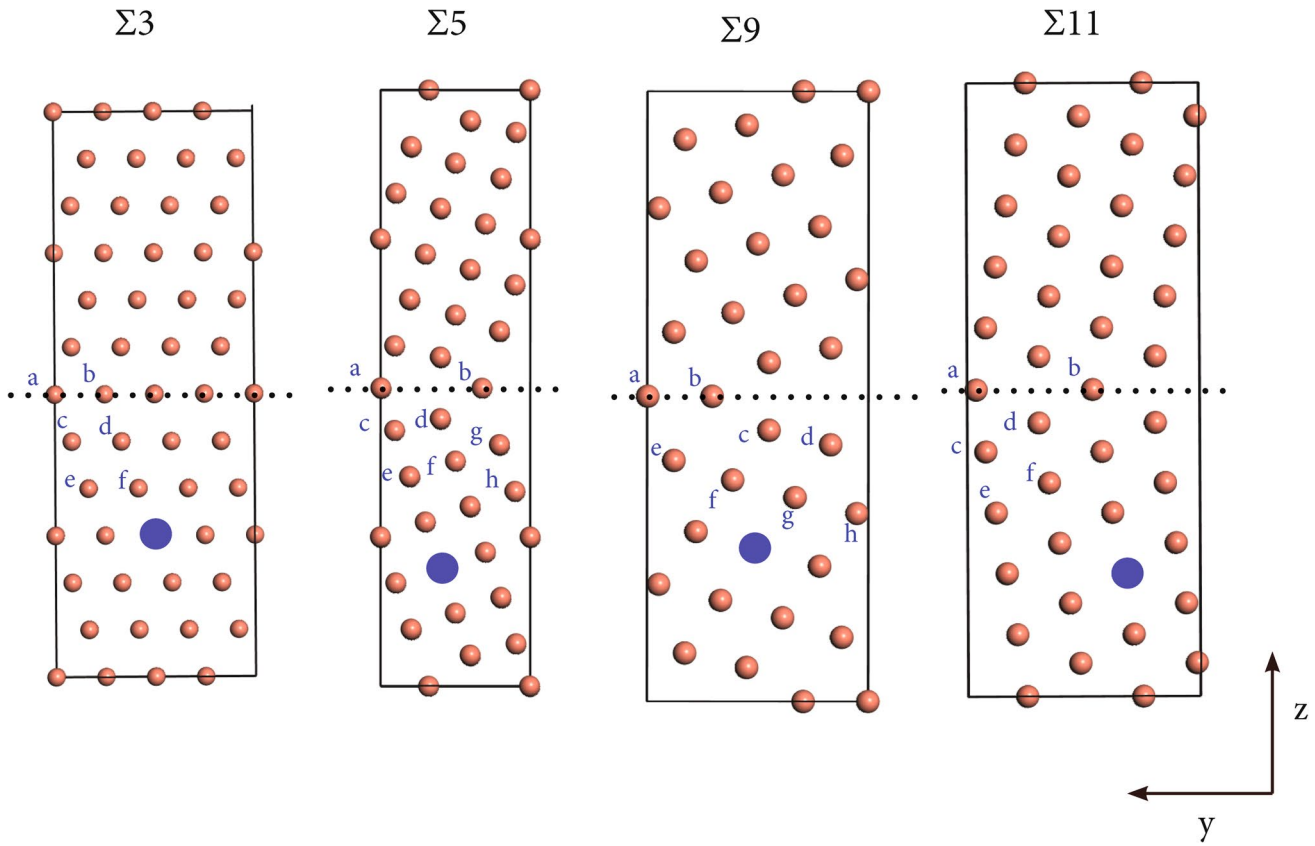

Figure 6 Supercells delimited by black lines with the geometry optimized Σ3, Σ5, Σ9 and Σ11 GB models. The dashed lines mark the GB atoms of the interface between the two planes. The absorption of P and S was investigated at the labelled sites. The dark blue atoms highlight the bulk reference site used to determine the segregation energies.

Table 2 Segregation energies (ΔE_{seg}) for P and S at Σ9 grain boundaries. Values for Σ3, Σ5 and Σ11 have been presented before in Table 1 in [8]

GB type	Segregation site	Pair	ΔE_{seg} (eV)		Coordinates (fractional)			Distance from GB (Å)
		q	P	S	x	y	z	
9	a	1	− 0653	− 0.724	0	0.004	0.5	0
9	b	1	0.009	− 0.335	0.25	0.29	0.5	0
9	c	2	− 0.493	− 0.655	0	0.606	0.443	1.248
9	d	2	− 0.274	− 0.384	0.333	0	0.421	1.716
9	e	2	− 0.276	− 0.562	0	0.192	0.392	2.36
9	f	2	− 0.243	− 0.274	0.25	0.5	0.363	2.972
9	g	2	0.065	0	0.25	0.102	0.34	3.488
9	h	2	0.013	0	0.25	0.102	0.315	4.015

Columns 4 to 9 are given with 3 decimals (trailing zeros are omitted)

for segregation decreases with increasing distance from the GB plane. Some positions at the GB plane are an exception to this. This happens because the strength of the bonds between the impurities and the Cu matrix is the result of a fine balance between excess volume and asymmetry of the binding site. The preferred symmetry and volume for the P and S

atoms at the binding sites are different. At distances from the GB plane exceeding 4.2 Å, the driving force for segregation is quite small, the ΔE_{seg} are larger than − 0.01 eV and bulk conditions may be expected.

Σ3 and Σ11 boundaries give smaller absolute values of ΔE_{seg} than Σ5 and Σ9. There is only one exception. This is believed to be a result of the more "open" structure for Σ5 and Σ9 than for Σ3 and Σ11. The open structure of Σ5 is well established in the literature [29]. It is evident that Σ9 is equally open. Since Σ9 is much more common than Σ5 in the canister material this is an important observation. The computed binding energies for S and P increase in magnitude when Σ9 is included.

Modelling occupancy of dopants in the grain boundaries

As shown above, the various GB types are associated with different segregation energies for alloying and impurity elements. P and S have quite different roles in the canister. P is an added element that increases the creep strength and ductility of copper. Even minor amounts dramatically reduce the climb rate of dislocations and thereby increase the creep strength [3, 4]. It also strongly enhances the creep ductility that is vital for the copper canisters for storage of spent nuclear fuel [5]. The segregation energies of P at the GBs are a critical factor for the creep ductility [6]. S on the other hand is an impurity element that reduces the creep ductility if the content is not well controlled [30].

A model for segregation energies is presented in detail in [8] and only the results of its derivation are shown here. The fraction of atomic sites x_{XGB} (occupancy) in and around the GBs that are filled by X atoms (X = S or P) is given by

$$x_{XGB} = x\exp(-\Delta\overline{E}_{Xseg}/kT) = x\sum_i \frac{p_i \exp(-\Delta E_{Xseg(i)}/kT)}{1 + x\exp(-\Delta E_{Xseg(i)}/kT)} \quad (1)$$

x is the concentration of P and S in the material expressed in moles, p_i is the frequency of occurrence of the different GB types and sites, $\Delta E_{Xseg(i)} < 0$ is the segregation energy at site i, $\Delta\overline{E}_{Xseg}$ is the average segregation energy, k and T are the Boltzmann constant and the absolute temperature, respectively. From Eq. (1), an expression for the average segregation energy can be obtained

$$\Delta\overline{E}_{Xseg} = -kT\ln\left(\sum_i \frac{p_i \exp(-\Delta E_{Xseg(i)}/kT)}{1 + x\exp(-\Delta E_{Xseg(i)}/kT)}\right) \quad (2)$$

The values used for the P and S concentration are x_P = 123 and x_S = 6 at. ppm that are typical values for the canister copper [6]. The values for $\Delta E_{Xseg(i)}$ and the frequency factors p_i for the GB types are those in Fig. 3 combined with the pair value q in Table 2. In comparison to the previous study [8], there are here two major differences. (i) Σ9 is directly considered. (ii) In the previous study, literature data for the distribution of GB types was used [29] with quite a different frequency of occurrence of the CSL compared to that in Fig. 3. This has effects in the results of the model for segregation energies as shown below.

The derived average segregation energies are presented in Fig. 7 for P and S in the canister. The values are computed in two different ways: (1) only values for Σ5, Σ7, Σ9 and Σ11 are included; (2) the influence of the remainder of all the GBs is estimated by assuming that they have about the same properties as Σ11.

The absolute value of the average segregation energies increases with increasing temperature. The trend is the same for tube and lid material, but the absolute value is slightly higher for the lid material. The lid material has a small amount of cold deformation (2–3%) [31]. It is known that cold work increases the Σ9 fraction of boundaries, Fig. 3. The two alternative ways to assess the average segregation energy yield similar results. A comparison is made to the previously published values where Σ9 was not included [8]. Due to the strong segregation effect for Σ9, the absolute values of the segregation energies are significantly larger in the present study. Results are shown in Fig. 8 for the P and S occupancy in the GBs.

The P and S occupancies decrease with increasing temperature in a similar way for tube and lid material, although the values for the lid are larger due to the higher absolute segregation energies in particular for S. The two alternative ways of modelling the P occupancy give again approximately the same results. That the difference between these two modelling alternatives is considerably smaller than in the previous analysis [8] illustrates the importance of including the Σ9 GB in the analysis. This also raises the occupancy of both P and S in relation to the previous study. Notice that the concentration of elements at the GBs is not very different for P and S despite the large difference in bulk concentrations. The relative increase in content

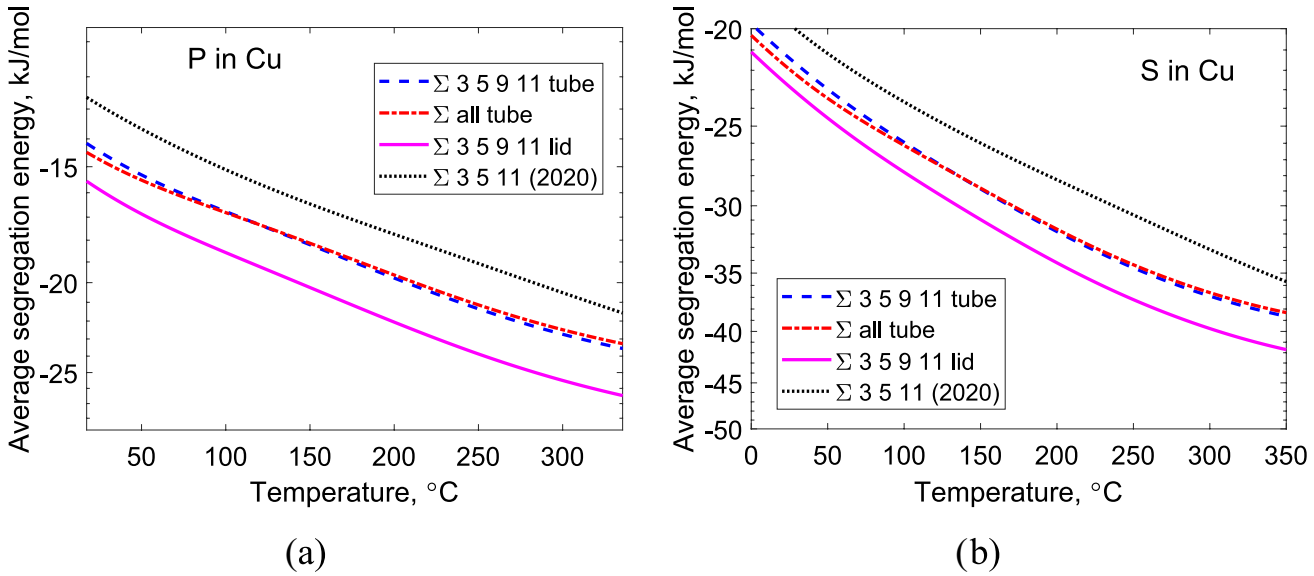

Figure 7 Average segregation energy for P and S at GBs in Cu versus temperature according to Eq. (2). For the dashed curve and the full drawn curve only Σ3, Σ5, Σ9 and Σ11 are taken into account. For the dashed-dotted curve (tube) also other GB types between Σ7 and Σ27 are included assuming the same segregation energies as for Σ11. Σ3 5 11 (2020) refers to previously published values [8]; (**a**) phosphorus; (**b**) sulphur.

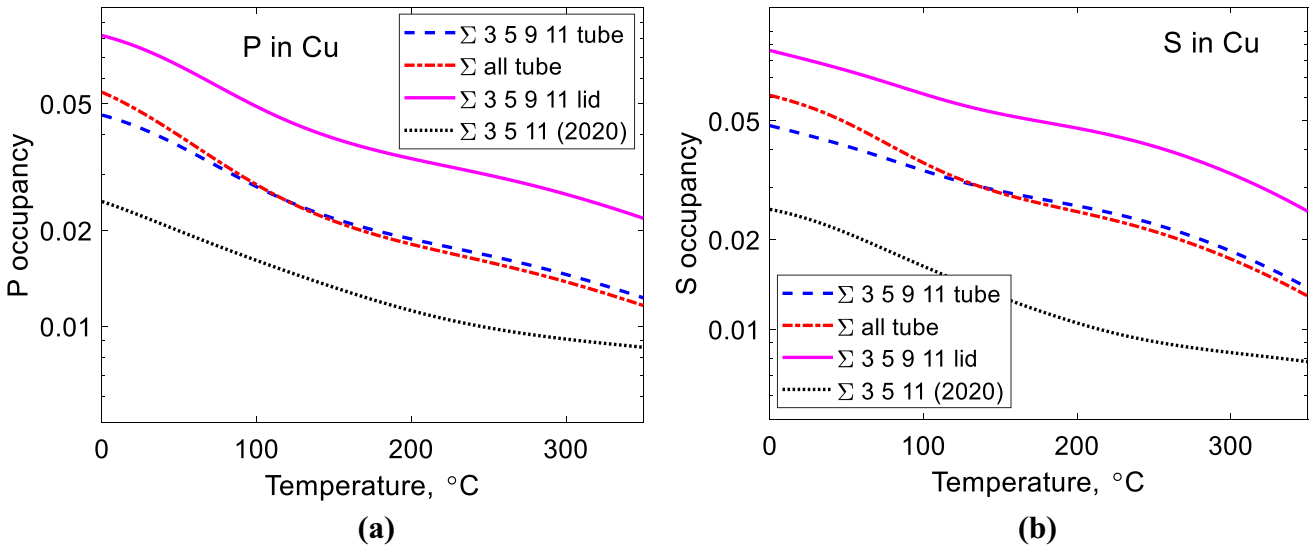

Figure 8 Computed occupancy of **a** P and **b** S at GBs in Cu versus temperature according to Eq. (1). For the dashed curve and the full drawn curve, only Σ3, Σ5, Σ9 and Σ11 are considered. For the dashed-dotted curve (tube) also other GB types between Σ7 and Σ27 are taken into account assuming the same segregation energies as for Σ11. Σ3 5 11 (2020) refers to previously published values [8]

at the GB is consequently much larger for S than for P. The difference between the tube and lid material illustrates that microstructure plays an important role for the properties of the corresponding section of the canister.

Cavity formation and creep ductility

It has been shown that Cu-OFP has a much better creep ductility than Cu-OF [5, 32]. Since good creep ductility is vital for the safety of the canisters, Cu-OFP has been selected as the canister material [33]. The creep ductility is controlled by the formation of creep cavities in the GB during brittle creep rupture. The cavities gradually grow and link to create cracks that lead to intercrystalline brittle rupture [5]. In many materials, cavity nucleation takes place at particles in the GBs. However, in oxygen-free copper, the number of particles in the GBs is so low that cavities in such positions would be insignificant. Instead, it is believed that the creep cavities are formed at GB-subboundary junctions. This case has been accurately modelled by Lim [34], who showed that the creation of cavities can give rise to a gain in free energy. It has been demonstrated that this model can quantitatively explain the influence of phosphorus on the creep ductility [6].

Creep cavities are believed to be initiated by grain boundary sliding, i.e. the movement of neighbouring lattices along their common boundary. The amount of GBS is given by [35]

$$\mu_{GBS} = \frac{3 r_{GBS} d_g \varepsilon}{2\xi} = C_s \varepsilon \tag{3}$$

where $r_{GBS} = 0.2$ is a constant, d_g the linear intercept grain size, $\xi = 1.36$ a geometric factor and ε the creep strain. C_s is a grain size dependent constant. It also appears in the expression for the number of creep cavities n_{cav} formed per unit GB area [36]

$$n_{cav} = \frac{0.9 C_s}{d_{sub}} \left(\frac{g_{sub}}{d_{sub}^2} + \frac{g_{part}}{\lambda^2} \right) \varepsilon = B_s \varepsilon \tag{4}$$

where d_{sub} is the subgrain size and λ is the interparticle spacing in the GB. g_{sub} and g_{part} are the fraction of the subgrain corners where cavities are formed. The expression for growth of the cavity radius R_{cav} is also needed to describe cavitation

$$\frac{dR_{cav}}{dt} = 2 D_0 K_f (\sigma - \sigma_0) \frac{1}{R_{cav}^2} \tag{5}$$

where t is the time, σ the applied stress, σ_0 the sintering stress and D_0 a constant proportional to the grain boundary self-diffusion coefficient. K_f depends on the area fraction of cavities. With the help of Eqs. (4) and (5), the area fraction of cavities A_f can be determined. Ductile rupture occurs if the prescribed value of elongation (of 0.4) is reached before A_f has reached a critical level (of 0.25). Otherwise the rupture is brittle.

The details for computing the creep ductility are given in [8] and are only briefly summarized here. The first step in predicting the creep ductility is to compute the creep deformation, which is based on climb of dislocations. A basic model for the creep deformation was developed some years ago [37] and it is described in several papers. The basic model that does not involve any adjustable parameters has been very successful and can quantitatively describe the creep deformation at low and high stresses and at low and high temperatures in copper [38]. The next step is to use Eqs. (3)–(5) to compute the amount of cavitation and the cavitated area fraction in the GBs. When the cavitated area fraction has reached a certain value, brittle creep rupture is assumed to occur. The computed creep deformation at failure is the creep ductility.

One aspect of the modelling is entirely new: the influence of the grain size on the creep ductility. As is evident from Eq. (3), there is a grain size dependence in the expression for the GBS. Equation (3) has recently been compared with available data in the literature [35]. It was found that both the strain and the grain size dependences were consistent with the analysed 650 data points. Since the constant C_s appears also in Eq. (4) for the number of nucleated cavities, it should be possible to compute its grain size dependence and also its influence on the ductility.

Since the modelling of the influence of grain size on the creep ductility is new, it will first be compared to literature data. Data for Cu-OF from [39] will be used. The influence of grain size at 475 °C is illustrated in Fig. 9. It is clear that the model can reproduce the observations reasonably well. According to Eqs. (3) and (4), the number of cavities decreases linearly with the grain size. With increasing grain size, a large decrease in the creep ductility can be anticipated. This is also what is observed.

For the canister material Cu-OFP, there are several aspects to investigate concerning creep ductility: (i) the distribution of CSL GBs; (ii) the binding of P to the GBs; (iii) the grain size distribution. The first two were investigated in a previous paper [8]. However, the distribution of the CSL GBs was taken from the literature, and it has turned out to be quite different from the distribution measured for the canister material. For example, Σ9 is much more common in the new measurements. Since it has an open structure, it

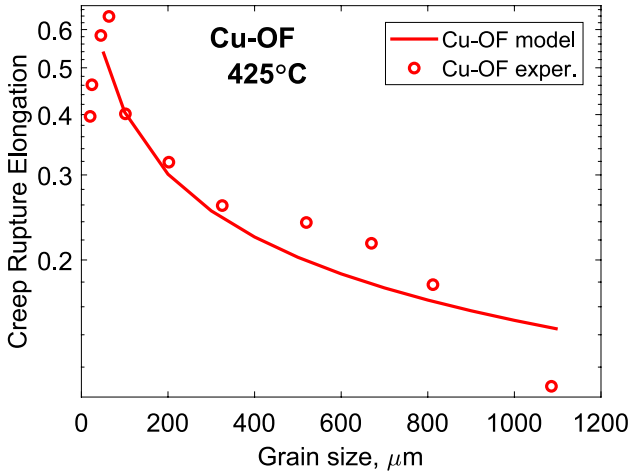

Figure 9 Creep rupture elongation versus grain size for oxygen-free copper Cu-OF at 425 °C. Experimental data from [39].

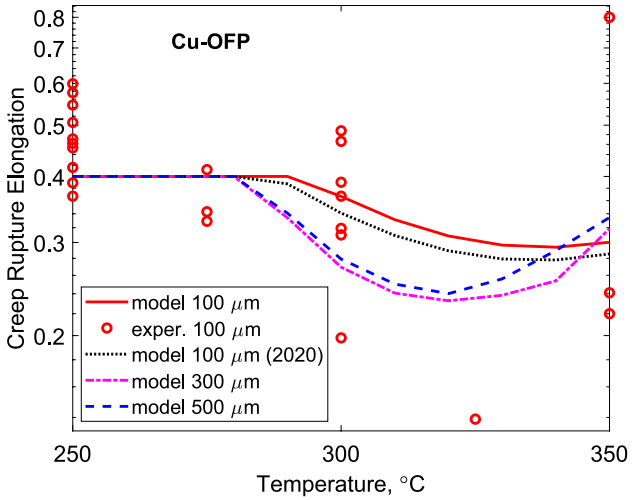

Figure 10 Creep rupture elongation versus temperature for oxygen-free copper with P, Cu-OFP at three grain sizes 100, 300 and 500 μm. Experimental data for grain sizes around 100 μm [5]. For comparison results from a previous study are given [8].

is quite efficient in segregating P atoms. This increases the absolute value of the segregation energy (Fig. 7a), and raises the P occupancy (Fig. 8a). This is expected to raise the creep ductility. This is also precisely what is found. In Fig. 10, the new results for the creep ductility are compared to the previously published values. The new values represent an increase, although small.

The modelled influence of the grain size is shown in Fig. 10. An increase in the grain size reduces the creep ductility, but only to a certain extent. The minimum ductility is at a grain size of 300 μm. For larger grain sizes, there is small increase. Larger grain sizes than 500 μm have been analysed. However, the difference from the situation at 500 μm is small. The reason for this behaviour is that the number of cavities reaches a saturation level. It is assumed that there is at most one cavity in each subgrain corner in agreement with observations, and these positions are quickly filled for larger grain sizes.

Discussion

Material for a copper canister for encapsulation of spent nuclear fuel has been investigated. The grain size distribution and GB structure have been analysed. The occurrence of CSL has been characterized. CSL boundaries were found to be more common than random high angle boundaries as shown in Fig. 4. This is assumed to improve properties related to corrosion [2]. Twin boundaries of the Σ3 type are by far the most common ones. The other $\Sigma 3^n$ boundaries (Σ9 and Σ27) have a higher frequency of occurrence than the remainder, which is in agreement with earlier findings. The presence of Σ9 and Σ27 is more pronounced in the lid material than in the tube wall. This is due to a remaining strain (2–3%) from the forging process.

The fraction of CSL boundaries in the canister tube and the lid is about 60 and 65%, respectively. This is about the same order as for grain boundary engineered (GBE) material [9]. It is evident that the different steps in the hot working of the canister have a positive effect in this respect. This is most obvious for the lid that is forged in several steps and annealed between some of these steps. This is agreement with the observations that hot working can be used to realize GBE [40, 41].

It has been suggested that it is not only the fraction of CSL boundaries that is of importance for the improvement of properties during GBE. The presence of annealing twins has also an effect [2]. It is evident from Fig. 1 that there are plenty of annealing twins in the canister material. Another effect arises if CSL boundaries meet at a triple point. It is believed that this reduces the progress of some intercrystalline failures [2]. However, this type of encounter does not seem frequent in the canister copper, see Fig. 1.

The canister copper is characterized by a broad distribution of grain sizes as shown in Fig. 4. Since the CSL boundaries have a higher occurrence than the random high angle GBs, the grain size increases dramatically if the former boundaries are excluded. The grain size is larger in the lid than in tube wall. It was found that the canister wall material was homogeneous, and the variation in CSL fractions and grain sizes was not very large. Some variation in grain size was found in the thickness direction in the canister wall. For example, close to the canister wall, the fraction of extra-large grains was higher, i.e. grains with diameters over 500 μm.

The top-sealing lid material shows significant differences in misorientation distribution, CSL fractions and grain size compared to the canister wall material. The canister wall material was completely recrystallized. It did not show many low angle GBs or other signs typical for deformed material. The lid material was not completely recrystallized. Significant amounts of low angle boundaries were present.

The distribution of CSL boundaries has been used to create the correct GB models to subsequently compute the binding energies for P and S to the GBs using quantum mechanical calculations. Almost every atomic site at and next to the CSL boundaries gives negative segregation energy indicating that a driving force for segregation exists, and that the impurities bind to the GBs up to distances of ≈ 4 Å from the GB planes. The role of Σ9 is significant. First, it is a frequently occurring GB. Secondly, it has an open structure that enhances the segregation. From the segregation energies the occurrence of impurities and dopants at the GBs can be determined.

The presence of P at the GBs is a vital quantity for the computation of the creep ductility. It is demonstrated, in agreement with previous studies that the P content increases the creep ductility significantly [6, 8]. In fact, it is shown that creep ductility is slightly increased when a more correct set of CSL boundaries as used in this investigation is taken into account. This is because the magnitudes of the binding energies for P are increased.

The effect of the grain size on the creep ductility has been analysed. The model for the amount GBS is linear in the grain size. This dependence has recently been verified by comparison to the available data for GBS in the literature [35]. Since the number of cavities is proportional to the amount of GBS, their dependence on the grain size is also known. That the ductility model can describe the influence of grain size well was verified by comparison to literature data for Cu-OF [39]. For the canister material Cu-OFP, the creep ductility was initially reduced when the grain size was increased. However, a minimum level was obtained at a grain size of 300 μm. A further increase in the grain size raised the ductility. This is due to a saturation effect for the number of nucleated cavities.

Conclusions

- In both the lid and the canister tube, the average grain size was 70 μm. The area weighted grain size in the lid was 200 μm, which was larger than in the canister tube, where it was 130 μm.
- The canister tube was extruded and completely recrystallized, whereas the lid was forged and had small amounts of non-recrystallized materials. As a consequence, the lid contained more lower angle boundaries (20%) than the canister (3%). This also resulted in a higher fraction of Σ9 boundaries in the lid.
- The frequency of CSL grain boundaries in the canister copper is 60% in the tube and 65% in the lid. These fractions are of the same order as in grain boundary engineered (GBE) materials, where the material has typically been exposed to several steps of cold work and annealing.
- The frequency of occurrence of the different CSL GBs in the material is an essential parameter to construct the correct models of the GBs that represent the real material for modelling with quantum mechanical or other atomic-scale methods.
- With the atomic structure and segregation energies determined for the CSL boundaries Σ3, Σ5, Σ9 and Σ11 with quantum mechanics methods, average segregation energies for P and S were evaluated. From these average energies, the occurrence of the dopants in the GBs was determined. The occurrence of P and S was found to be higher than in a previous study, mainly due to the inclusion of Σ9 in the analysis. This is a common GB and leads to large segregation energies.
- The creep ductility is improved by higher P content in the GBs. In particular, the open structure of the Σ9 GB allows the segregation of more P atoms per unit of GB area than for most of the other GBs. The model for the creep ductility is improved in relation

to the previous study although the raise in ductility is small.
- The number of creep cavities is modelled to be proportional to the grain size. Since it is likely that this is the first time that influence of the grain size on the creep ductility is modelled, the approach was first verified for literature data for Cu-OF. In spite of a large variation with grain size, and a large reduction with increasing grain size, the data could be well described. Then, the model was applied to Cu-OFP. When the grain size was increased to 300 μm, there was a drop in the ductility. But further increase in the grain size did not reduce the ductility anymore. The reason is believed to be a saturation in the number of creep cavities for large grain sizes.

Acknowledgements

Financial support from Swedish Nuclear Fuel and Waste Management Co (SKB) is gratefully acknowledged, grant 4501773898 and 4501773874. The authors want to thank Christina Lilja, SKB for her continuous support and valuable suggestions during the work. The computations were performed on resources provided by the National Academic Infrastructure for Supercomputing in Sweden (NAISS), at the PDC Centre for High Performance Computing at KTH—Royal Institute of Technology, Stockholm, partially funded by the Swedish Research Council through grant agreements no. 2022-06725.

Author contributions

Joacim Hagström was involved in experiments, microscopy and writing manuscript. Rolf Sandström contributed to conceptualization, methodology, modelling and writing manuscript. Cláudio M. Lousada was involved in DFT modelling and writing manuscript.

Funding

Open access funding provided by Royal Institute of Technology.

Data availability

The data that have been used are confidential.

Declarations

Conflict of interest The authors declare that they have no known competing financial interests or personal relationships that could have appeared to influence the work reported in this paper.

Ethical approval Not applicable.

References

[1] Sutton AP, Balluffi RW (1996) Interfaces in crystalline materials. Oxford University Press, Oxford
[2] Randle V (2010) Grain boundary engineering: an overview after 25 years. Mater Sci Technol 26:253–261
[3] Sandstrom R, Andersson HCM (2008) The effect of phosphorus on creep in copper. J Nucl Mater 372:66–75
[4] Sandstrom R, Andersson HCM (2008) Creep in phosphorus alloyed copper during power-law breakdown. J Nucl Mater 372:76–88
[5] Sandström R, Wu R (2013) Influence of phosphorus on the creep ductility of copper. J Nucl Mater 441:364–371
[6] Sandström R, Wu R, Hagström J (2016) Grain boundary sliding in copper and its relation to cavity formation during creep. Mater Sci Eng A 651:259–268

[7] Lousada CM, Korzhavyi PA (2022) Single vacancies at Σ5, Σ9 and Σ11 grain boundaries of copper and the geometrical factors that affect their site preference. J Phys Chem Solids 169:110833–110840
[8] Sandström R, Lousada CM (2020) The role of binding energies for phosphorus and sulphur at grain boundaries in copper. J Nucl Mater 544:152682–152691
[9] Randle V (2004) Twinning-related grain boundary engineering. Acta Mater 52:4067–4081
[10] Randle V, Buschow KHJ, Cahn RW, Flemings MC, Ilschner B, Kramer EJ, Mahajan S, Veyssière P (2005) Grain boundary engineering, in Encyclopedia of materials: science and technology. Elsevier, Oxford, pp 1–8
[11] Michiuchi M, Kokawa H, Wang ZJ, Sato YS, Sakai K (2006) Twin-induced grain boundary engineering for 316 austenitic stainless steel. Acta Mater 54:5179–5184
[12] Tan L, Sridharan K, Allen TR, Nanstad RK, McClintock DA (2008) Microstructure tailoring for property improvements by grain boundary engineering. J Nucl Mater 374:270–280
[13] Reed BW, Kumar M, Minich RW, Rudd RE (2008) Fracture roughness scaling and its correlation with grain boundary network structure. Acta Mater 56:3278–3289
[14] Tan L, Sridharan K, Allen TR (2007) Effect of thermomechanical processing on grain boundary character distribution of a Ni-based superalloy. J Nucl Mater 371:171–175
[15] Bechtle S, Kumar M, Somerday BP, Launey ME, Ritchie RO (2009) Grain-boundary engineering markedly reduces susceptibility to intergranular hydrogen embrittlement in metallic materials. Acta Mater 57:4148–4157
[16] Coleman M, Randle V (2008) Changes in interface parameters and tensile properties in copper as a consequence of iterative processing. Metall Mater Trans A 39:2175–2183
[17] Lee DS, Ryoo HS, Hwang SK (2003) A grain boundary engineering approach to promote special boundaries in Pb-base alloy. Mater Sci Eng A 354:106–111
[18] Kumar M, Schwartz AJ, King WE (2002) Microstructural evolution during grain boundary engineering of low to medium stacking fault energy fcc materials. Acta Mater 50:2599–2612
[19] Yang X, Wang P, Huang M (2022) Grain boundary evolution during low-strain grain boundary engineering achieved by strain-induced boundary migration in pure copper. Mater Sci Eng A. https://doi.org/10.1016/j.msea.2021.142532
[20] Randle V, Owen G (2006) Mechanisms of grain boundary engineering. Acta Mater 54:1777–1783
[21] Randle V (1999) Mechanism of twinning-induced grain boundary engineering in low stacking-fault energy materials. Acta Mater 47:4187–4196
[22] Hagström J (2023) Microstructure, crystallography and CSL grain boundaries in copper canisters for nuclear waste disposal, SKB TR-23-12, Swedish nuclear waste management company
[23] Lousada CM, Korzhavyi PA (2020) Segregation of P and S impurities to A Σ9 grain boundary in Cu. Metals 10:1–8
[24] Lousada CM, Korzhavyi PA (2024) Segregation of P and S to frequently occurring grain boundaries of Cu: single atoms and cooperative effects. J Phys Chem Solids 193:112124–112135
[25] Lousada CM, Korzhavyi PA (2023) Pathways of hydrogen atom diffusion at fcc Cu: Σ9 and Σ5 grain boundaries vs single crystal. J Mater Sci 44:17004–17018
[26] Randle V (2001) The coincidence site lattice and the 'sigma enigma.' Mater Charact 47:411–416
[27] Fortes MA (1972) Coincidence site lattices. physica status solidi (b) 54:311–319
[28] Luo Y-R, Luo Y-R (2007) Comprehensive handbook of chemical bond energies. CRC Press, Boca Raton
[29] Mishin OV, Gertsman VY, Gottstein G (1997) Distributions of orientations and misorientations in hot-rolled copper. Mater Charact 38:39–48
[30] Li Y, Korzhavyi PA, Sandström R, Lilja C (2017) Impurity effects on the grain boundary cohesion in copper. Phys Rev Mater 1:070602-1–070602-5
[31] Wu R, Pettersson N, Martinsson Å, Sandström R (2014) Cell structure in cold worked and creep deformed phosphorus alloyed copper. Mater Charact 90:21–30
[32] Henderson PJ, Sandstrom R (1998) Low temperature creep ductility of OFHC copper. Mater Sci Eng A 246:143–150
[33] Rosborg B, Werme L (2008) The Swedish nuclear waste program and the long-term corrosion behaviour of copper. J Nucl Mater 379:142–153
[34] Lim LC (1987) Cavity nucleation at high temperatures involving pile-ups of grain boundary dislocations. Acta Metall 35:1663–1673
[35] He J-J, Sandström R, Lü S-R, Korzhavyi P, Zhang J, Qin H-Y, Liu J-B (2025) Predicting grain boundary sliding in metallic materials. Acta Mater. https://doi.org/10.1016/j.actamat.2025.120718
[36] Sandström R (2024) Cavitation. In: Basic modeling and theory of creep of metallic alloys. Springer Series in Materials Science, p. 185–203
[37] Sandstrom R (2012) Basic model for primary and secondary creep in copper. Acta Mater 60:314–322
[38] Sandström R (2023) Primary creep at low stresses in copper. Mater Sci Eng A 873:144950–144958
[39] Fleck RG, Cocks GJ, Taplin DMR (1970) The influence of polycrystal grain size upon the creep ductility of copper. Metall Trans 1:3415–3420

[40] Liu T, Xia S, Du D, Bai Q, Zhang L, Lu Y (2019) Grain boundary engineering of large-size 316 stainless steel via warm-rolling for improving resistance to intergranular attack. Mater Lett 234:201–204

[41] Souaï N, Bozzolo N, Nazé L, Chastel Y, Logé R (2010) About the possibility of grain boundary engineering via hot-working in a nickel-base superalloy. Scripta Mater 62:851–854